Fuel Cells

DOI: 10.1002/anie.200801667

A Proton-Conducting Fuel Cell Operating with Hydrocarbon Fuels

*Pilwon Heo, Kenichi Ito, Atsuko Tomita, and Takashi Hibino**

It is commonly believed that hydrogen is the most ideal fuel for fuel cells because it has the highest energy conversion efficiency and the most environmentally friendly properties among the various possible fuels. Nearly half of the chemical energy of hydrogen and oxygen is actually converted into electricity with only water as a product. However, well-to-wheels (WTW) analyses are necessary to evaluate fuel-cell systems since the energy and environmental benefits of hydrogen as a fuel strongly depend on the choice of hydrogen production pathways. Indeed, the benefits of fuel-cell vehicles using hydrogen as fuel are not so great if hydrogen is produced from fossil fuels.[1–3] This is mainly because of the energy loss in steam reforming hydrocarbons at high temperatures. Additional energy losses result from hydrogen storage and purification, a problem common to all hydrogen production pathways.

Direct utilization of hydrocarbons in fuel cells can be expected to significantly improve their WTW efficiency.[4,5] Indeed, solid oxide fuel cells (SOFCs) that use methane show higher WTW efficiencies ($\approx 50\,\%$) than polymer electrolyte fuel cells (PEFCs) with gases reformed from methane ($\approx 30\,\%$).[6] However, SOFCs present a number of inherent challenges for transport applications, such as low mechanical strength, slow start-up time, and serious anode deterioration.[7] The first two challenges are crucial for fuel-cell vehicles. The development of PEFCs to meet this challenge has also been attempted, but some serious challenges remain, including low open-circuit voltages (OCVs), poor cell performance, and high Pt loadings.[8,9] This is because operating temperatures below 100 °C are too low to achieve sufficiently high reaction activity at the anode.

We report herein the investigation of the direct oxidation of hydrocarbon fuels, including methane, ethane, propane, and butane, over Pt-free anodes in a proton-conducting fuel cell (PCFC) in the temperature range 100–300 °C. In^{3+}-doped SnP_2O_7 shows high proton conductivities above 10^{-1} S cm^{-1} over this temperature range (see the Supporting Information).[10] This material has also been explored for use as an electrolyte in intermediate-temperature fuel cells, which are characterized by excellent thermal stability up to 300 °C and a high tolerance towards CO.[11] Another important characteristic is that these fuel cells allow the use of transition-metal carbides as alternative anode materials to platinum.[12] The present results demonstrate that these characteristics can successfully address the challenges encountered in SOFCs and PEFCs. The PCFCs used here consisted of M_xC/C (M = Mo, W, Nb, V, and Ti, 30 mg M_xC per cm^2) | $Sn_{0.9}In_{0.1}P_2O_7$ | Pt/C (0.6 mg Pt per cm^2). X-ray diffraction (XRD) patterns of these anode materials showed that each metal carbide existed as a single phase (see Figure S1 in the Supporting Information). Polarization measurements were carried out after supplying the fuel chamber with a mixture of propane and water vapor. The Mo_2C/C anode exhibited the best performance for propane oxidation (Figure 1). Mo_2C has catalytic

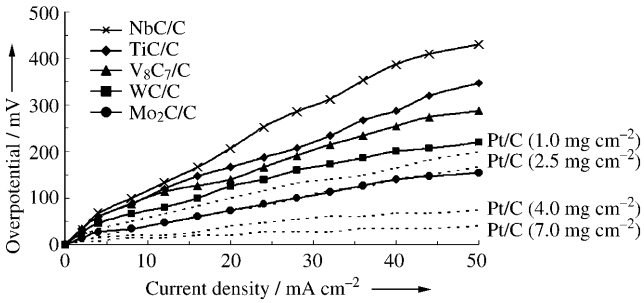

Figure 1. Overpotentials of various anodes for propane oxidation at 300 °C. The loading of the carbides was 30 mg cm^{-2}. A mixture of propane (7 vol %) and water vapor (42 %) in argon was supplied into the anode chamber at 60 mL min^{-1}.

characteristics similar to those of platinum-group metals, its catalytic activity is explained by the change in the electron density of the d band of Mo upon carburization: the introduction of C atoms into the Mo metal lattice causes a contraction of the d band, and thus enhancing the d-electron density to the d-electron density levels of Pt.[13] However, the performance of Mo_2C/C was still somewhat inferior to that of Pt/C (Figure 1); the overpotential value of Mo_2C/C was 154 mV at 50 mA cm^{-2}, which was lower than those of Pt/C with Pt loadings of 1.0 and 2.5 mg cm^{-2}, but higher than those of Pt/C with Pt loadings of 4.0 and 7.0 mg cm^{-2}. Our previous study showed that the hydrogen oxidation activity of Mo_2C was improved by impregnating a molybdenum salt, $(NH_4)_6Mo_7O_{24}\cdot 4H_2O$, with a zirconium salt, $ZrCl_2O\cdot 8H_2O$, and then carburizing the impregnated sample in the same manner as Mo_2C.[12] Zirconium-modified Mo_2C/C had a similar effect on hydrocarbon oxidation (Figure 2a); the overpotential for propane oxidation decreased with increasing content of Zr species and reached a minimum at a Mo_2C:ZrO_2 weight ratio of 0.8:0.2. The minimum overpotential value was 60 mV at 50 mA cm^{-2}, which was approx-

[*] Dr. P. Heo, K. Ito, Prof. Dr. T. Hibino
Graduate School of Environmental Studies, Nagoya University
Furo-cho, Chikusa-ku, Nagoya 464-8601 (Japan)
Fax: (+81) 52-789-4206
E-mail: hibino@urban.env.nagoya-u.ac.jp
Dr. A. Tomita
National Institute of Advanced Industrial
Science and Technology (AIST)
Simosidami, Moriyama-ku, Nagoya 463-8560 (Japan)

Supporting information for this article is available on the WWW under http://dx.doi.org/10.1002/anie.200801667.

imately one-third of the overpotential of untreated Mo_2C/C. The XRD profile of Zr-modified Mo_2C/C revealed that the added Zr species was present as ZrO_2 (Figure 2b). In addition, the Mo_2C diffraction peaks did not shift upon the addition of ZrO_2 to the catalyst, which suggested that Zr was not incorporated into the Mo_2C crystalline lattice. The Scherrer formula was applied to estimate the Mo_2C particle size, which was seen to attain a minimum at a Mo_2C:ZrO_2 weight ratio of 0.8:0.2 (Figure 2a); the particle sizes were 28 nm and 14 nm for Mo_2C/C and Mo_2C-ZrO_2/C, respectively. A similar difference was observed in the Mo_2C particle size, as revealed by transmission electron microscopy (TEM) measurements of the two catalysts (Figure 2c); the TEM images showed that the Mo_2C particle sizes were smaller for Mo_2C-ZrO_2/C than for Mo_2C/C. These results indicate that the Mo_2C particles show a higher dispersion with ZrO_2 than without ZrO_2. It is likely that excessive sintering of Mo_2C during carburization is inhibited in the presence of ZrO_2, which results in the significantly improved catalytic activity of Mo_2C towards propane oxidation.

Fuel-cell tests were performed between 100 and 300 °C using propane as fuel (Figure 3a). The OCV increased with temperature until 200 °C and thereafter slightly decreased with temperature. The temperature dependence observed above 200 °C is consistent with the thermodynamic prediction suggesting that the anode potential is no longer limited by reaction kinetics under such conditions. However, the OCV value of 862 mV at 200 °C is lower than the theoretical value of 1080 mV. The lower OCV value is due to the physical leakage of gas through the electrolyte and partial electron-hole conduction in the electrolyte, as reported in previous studies.[10] The voltage drop was greatly reduced by elevating the temperature (Figure 3a). The resulting peak power density reached 53 mW cm^{-2} at 300 °C. There is not a large difference in peak power density between the Mo_2C-ZrO_2/C and Pt/C (7 mg Pt per cm^2) anodes; the peak power density for Pt/C at 300 °C was 60 mW cm^{-2} (see Figure S2 in the Supporting Information). More importantly, the OCVs observed for Mo_2C-ZrO_2/C are higher than those for Pt/C; the OCV for Pt/C at 300 °C is only 679 mV. This point will be discussed later. These results demonstrate that Mo_2C-ZrO_2/C is a promising anode catalyst for direct hydrocarbon fuel cells operating at intermediate temperatures.

The comparison of cell performance with various hydrocarbon fuels was conducted at 300 °C (Figure 3b). Although the OCV ranged between 790 and 850 mV for all the hydrocarbon fuels, the voltage drop depended quite strongly on the hydrocarbon species; the voltage drop decreased in the order butane < propane < ethane < methane. This corresponded to the anode overpotential order observed at the same temperature (see Figure S3 in the Supporting Information). Thus, the present fuel cell yielded its highest peak power density of 55 mW cm^{-2} with butane as the fuel. This suggests that higher hydrocarbon fuels are more desirable for the operation of this fuel cell, which is suited to transport applications since such fuels are easily stored.

To better understand the reaction of hydrocarbons at the anode, the products in the outlet gas from the fuel-cell anode at 300 °C were analyzed using an online gas chromatograph.

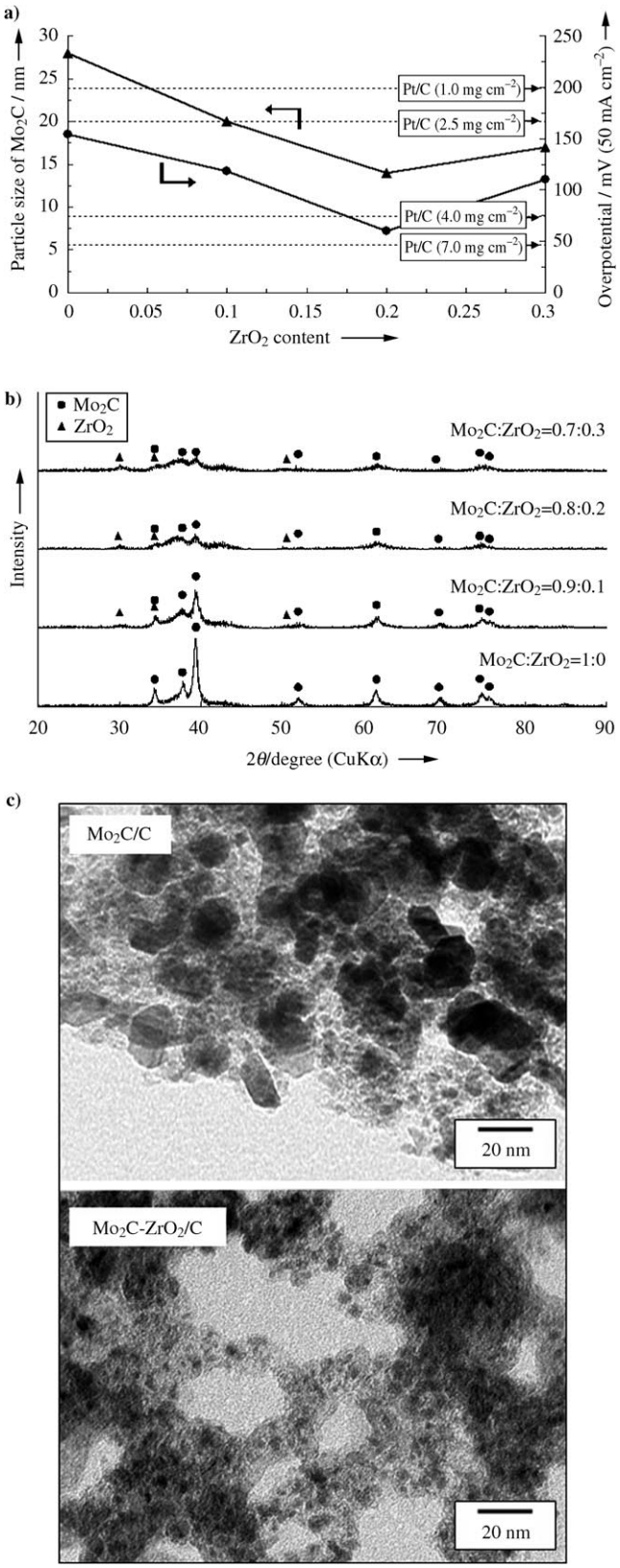

Figure 2. a) Particle size of Mo_2C and overpotential of Mo_2C–ZrO_2/C for propane oxidation as a function of ZrO_2 content in Mo_2C–ZrO_2/C. The overpotential of the Mo_2C–ZrO_2/C anode was measured under the same conditions as in Figure 1. b) XRD patterns of Mo_2C–ZrO_2/C with different proportions of ZrO_2. c) TEM micrographs of Mo_2C/C and Mo_2C–ZrO_2/C (Mo_2C:ZrO_2 = 0.8:0.2).

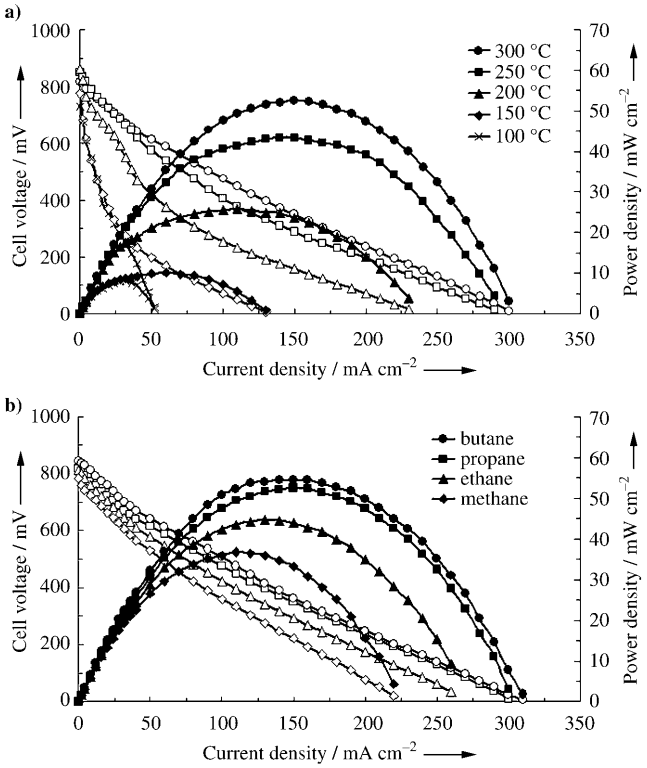

Figure 3. Cell voltage and power density versus current density for a fuel cell with a Mo_2C-ZrO_2/C anode (Mo_2C:ZrO_2 = 0.8:0.2). a) T = 100–300 °C, fuel = propane (7 vol %) and water vapor (42 vol %), flow rate = 60 mL min^{-1}, total pressure = 1 atm. b) T = 300 °C, fuel = methane (7 vol %) and water vapor (14 vol %), ethane (7 vol %) and water vapor (28 vol %), propane (7 vol %) and water (42 vol %) vapor, and butane (7 vol %) and water vapor (56 vol %), flow rate = 60 mL min^{-1}, total pressure = 1 atm.

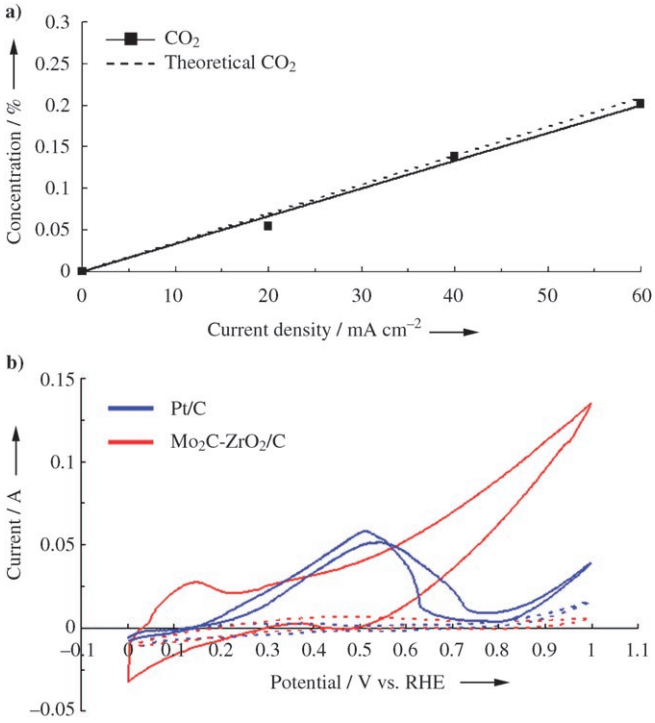

Figure 4. a) Product concentration for propane oxidation as a function of current density over a Mo_2C–ZrO_2/C anode at 300 °C. b) Cyclic-voltammetry (CV) profiles of Pt/C and Mo_2C–ZrO_2/C anodes in a mixture of propane and water vapor (solid line) and argon (dotted line) at 300 °C. The reference electrode was attached beside the counter electrode on the surface of the electrolyte and exposed to pure hydrogen.

No product was observed at the OCV for any of the hydrocarbons tested and CO_2 was the only constituent of the product gas during the cell discharge. The CO_2 concentration increased linearly with current density and approached the theoretical value of CO_2 concentration for 100 % faradic efficiency (Figure 4 a for propane and Figure S4 in the Supporting Information for other hydrocarbons). These results demonstrate that the hydrocarbons are converted directly into CO_2, with a current efficiency of approximately 100 %, according to the oxidation reaction shown in Equation (1).

$$C_nH_{2n+2} + 2n\,H_2O \rightarrow (6n+2)H^+ + (6n+2)e^- + n\,CO_2 \quad (1)$$

It has been reported that the oxidation product of a hydrocarbon on Pt in acidic solutions is CO_2, for which the reaction mechanism shown in Equations (2)–(5) is proposed (ads = adsorbed).[9,14]

$$(C_nH_{2n+2})_{ads} \rightarrow (C_nH_{2n+1})_{ads} + H^+ + e^- \quad (2)$$

$$(C_nH_{2n+1})_{ads} \rightarrow (C_1)_{ads} + (C_{n-1})_{ads} + x\,H^+ + x\,e^- \quad (3)$$

$$2\,H_2O \rightarrow 2(OH)_{ads} + 2\,H^+ + 2\,e^- \quad (4)$$

$$(C_1)_{ads} + 2(OH)_{ads} \rightarrow CO_2 + 2\,H^+ + 2\,e^- \quad (5)$$

The rate-determining step in the overall oxidation of the hydrocarbon to CO_2 is thought to be Equations (4) and (5), wherein the oxygen-containing species $(OH)_{ads}$, formed through the oxidation of water vapor, reacts with $(C_1)_{ads}$ to form CO_2. This mechanism is similar to that reported for methanol or CO oxidation in the presence of water.[15–17]

Cyclic voltammetry (CV) measurements allow us to understand the potential regions corresponding to Equations (4) and (5). For the Pt/C anode, the processes in Equations (4) and (5) occurred at E = 0.54 V in the positive-direction scan and the reaction in Equation (5) occurred, as before, at E = 0.51 V in the negative-direction scan (Figure 4 b). This means that the reaction in Equation (5) was inhibited by the strong adsorption of $(OH)_{ads}$ on the Pt surface at high potentials during the scan, and then restarted by the reduction of the strongly adsorbed $(OH)_{ads}$ upon scan direction reversal. Meanwhile, the CV profiles of the Mo_2C-ZrO_2/C anode showed the oxidation peak of the reactions in Equations (4) and (5) at E = 0.15 V during the positive-direction scan (Figure 4 b). This potential value is much lower than that observed for the Pt/C anode, which is consistent with the difference in OCV between the two anodes. Another important result is that the Mo_2C–ZrO_2/C anode has no peak potential corresponding to Equation (5) during the negative potential scan, in contrast to the Pt/C anode, which is indicative of a weak interaction between $(OH)_{ads}$ and the surface sites of the catalyst. Thus, it is assumed that the

turnover rate of the reaction in Equation (5) on the Mo_2C–ZrO_2/C anode is considerably higher than on the Pt/C anode.

The present results demonstrate that the direct oxidation of hydrocarbons no longer needs to be carried out above 300 °C. The operation of the fuel cell at 300 °C can reduce the start-up time as well as prevent carbon deposition on the anode surface. The formation of carbon from propane over a Ni/Al_2O_3 catalyst, one of the most active catalysts for coking, begins at 430 °C.[18] Another important result is that Mo_2C can be used in anodes for hydrocarbon oxidation. This is significant for the conversion of hydrocarbon fuels because Mo_2C shows high tolerance toward sulfidation[19] as well as carbon deposition.[20] However, the power densities obtained in this study are substantially lower than those reported for SOFCs.[1–3] One reason for this is the large thickness (1 mm) of the electrolyte used; additional work needs to be done to prepare thinner electrolyte films.

Experimental Section

Metal carbide anodes, M_xC/C (M = Mo, W, Nb, V, and Ti), were synthesized as follows. The corresponding metal salts (e.g., $(NH_4)_6Mo_7O_{24}\cdot 4H_2O$) were impregnated in a carbon support (Black Pearl, BET surface area: 1365 $m^2 g^{-1}$). The impregnated sample was reduced in a mixture of 10 vol% H_2 in Ar at 500 °C for 2 h and then carburized in a mixture of 20 vol% CH_4 in H_2 at a temperature between 700 and 1200 °C depending on the material (e.g., $T = 700$ °C for Mo_2C) for 3 h. The loading of all the carbides was 30 mg cm^{-2}. Pt/C anodes (30 wt% Pt/C, 1–7 mg Pt per cm^2, Black Pearl) were used for comparison. A Pt/C cathode (10 wt% Pt/C, 0.6 mg Pt per cm^2) was purchased from E-TEK, Inc. The microstructure of the catalysts was analyzed using X-ray diffraction (XRD, Shimadzu XRD-600) and transmission electron microscopy (TEM, Hitachi H-800).

$Sn_{0.9}In_{0.1}P_2O_7$ was prepared as reported previously.[10] SnO_2 and In_2O_3 powders were mixed with H_3PO_4 (85%) and deionized water and stirred at 300 °C until the mixture formed a highly viscous paste. The pastes were calcined in an alumina pot at 650 °C for 2.5 h and then ground with a mortar and pestle. Finally, the compound powders were pressed into pellets under a pressure of 2×10^3 kg cm^{-2}.

Electrode and cell performance measurements: The anode and cathode (area: 0.5 cm^2) were attached to opposite sides of the electrolyte (thickness: 1.0 mm; see Figure S5 in the Supporting Information). Two gas chambers were set up by placing the cell assembly between two alumina tubes. A mixture of hydrocarbon (methane, ethane, propane, or butane) and water vapor was supplied to the fuel chamber at a flow rate of 60 mL min^{-1} at ambient pressure. The pressure ratio of water to hydrocarbon was maintained at the stoichiometric composition in Equation (1): 7 vol% methane and 14 vol% water vapor; 7 vol% ethane and 28 vol% water vapor; 7 vol% propane and 42 vol% water vapor; 7 vol% butane and 56 vol% water vapor. Unhumidified air was supplied to the air chamber at a flow rate of 30 mL min^{-1}. The anodic polarization properties were measured by the current interruption method using a current pulse generator. For this measurement, an Au reference electrode was attached on the side surface of the electrolyte and exposed to ambient atmosphere. A constant current with a periodic off-pulse signal of 100 μs was applied between the anode and cathode, and the transient response of the anode potential was recorded using an oscilloscope. The potential components of the fast drop and slow decay were assigned to the IR (I: current density, R: electrolyte resistance) drop and overpotential, respectively. The overpotential was thus estimated by eliminating the IR drop from the anode potential. The cell performance was measured by using the four-probe method, wherein the ohmic resistance of the lead wires was negligible. The outlet gas from the fuel chamber was analyzed using online gas chromatography. The gas concentrations were obtained after the steady-state composition of the reaction was attained.

CV measurements: Another three-electrode arrangement was used with Au and Pt/C electrodes supplied with pure hydrogen as reference and counter electrodes, respectively (see Figure S6 in the Supporting Information). The CV profiles were collected between 0 and 1 V vs. reversible hydrogen electrode (RHE) at a scan rate of 10 mV s^{-1}.

Received: April 9, 2008
Revised: August 12, 2008

Keywords: catalysis · fuel cells · hydrocarbon fuels · molybdenum · zirconium

[1] M. Wang, *J. Power Sources* **2002**, 112, 307.
[2] M. Wietschel, U. Hasenauer, A. de Groot, *Energy Policy* **2006**, *34*, 1284.
[3] A. M. Svensson, S. Møller-Holst, R. Glöckner, O. Maurstad, *Energy* **2007**, *32*, 437.
[4] E. P. Murray, T. Tsai, S. A. Barnett, *Nature* **1999**, *400*, 649.
[5] S. Park, J. M. Vohs, R. J. Gorte, *Nature* **2000**, *404*, 265.
[6] Z. Zhan, S. A. Barnett, *Science* **2005**, *308*, 844.
[7] B. C. H. Steele, A. Heinzel, *Nature* **2001**, *414*, 345.
[8] O. Savadogo, F. J. Rodriguez, *J. New Mater. Electrochem. Syst.* **2001**, *4*, 93.
[9] W. S. Li, D. S. Lu, J. L. Luo, K. T. Chuang, *J. Power Sources* **2005**, *145*, 376.
[10] M. Nagao, A. Takeuchi, P. Heo, T. Hibino, M. Sano, A. Tomita, *Electrochem. Solid-State Lett.* **2006**, *9*, A105.
[11] P. Heo, H. Shibata, M. Nagao, T. Hibino, M. Sano, *J. Electrochem. Soc.* **2006**, *153*, A897.
[12] P. Heo, M. Nagao, M. Sano, T. Hibino, *J. Electrochem. Soc.* **2007**, *154*, B53.
[13] J. S. Choi, G. Bugli, G. Djega-Mariadassou, *J. Catal.* **2000**, *193*, 238.
[14] B. Brummer, J. I. Ford, M. J. Turner, *J. Phys. Chem.* **1965**, *69*, 3424.
[15] H. A. Gasteiger, N. Marković, P. N. Ross, E. J. Cairns, *J. Phys. Chem.* **1993**, *97*, 12020.
[16] T. Iwasita, H. Hoster, A. John-Anacker, W. F. Lin and W. Vielstich, *Langmuir* **2000**, *16*, 522.
[17] J. S. Spendelow, P. K. Babu, A. Wieckowski, *Curr. Opin. Solid State Mater. Sci.* **2005**, *9*, 37.
[18] S. Natesakhawat, R. B. Watson, X. Wang, U. S. Ozkan, *J. Catal.* **2005**, *234*, 496.
[19] D. J. Sajkowski, S. T. Oyama, *Appl. Catal. A* **1996**, *134*, 339.
[20] D. C. LaMont, A. J. Gilligan, A. R. S. Darujati, A. S. Chellappa, W. J. Thomson, *Appl. Catal. A* **2003**, *255*, 239.

